

# XMMSL1 J060636.2-694933: An XMM-Newton Slew discovery and Swift/Magellan follow up of a new Classical Nova in the LMC

A. M. Read<sup>1</sup> R. D. Saxton<sup>2</sup> P. G. Jonker<sup>3,4</sup> E. Kuulkers<sup>2</sup> P. Esquej<sup>1</sup> G. Pojmanski<sup>5</sup> M. A. P. Torres<sup>4</sup> M. R. Goad<sup>1</sup>  
M. J. Freyberg<sup>6</sup> M. Modjaz<sup>7</sup>

<sup>1</sup>Dept. of Physics and Astronomy, Leicester University, Leicester LE1 7RH, U.K.

e-mail: amr30@star.le.ac.uk

<sup>2</sup>XMM-Newton SOC, ESAC, Apartado 78, 28691 Villanueva de la Cañada, Madrid, Spain

<sup>3</sup>SRON, Netherlands Institute for Space Research, Sorbonnelaan 2, 3584 CA, Utrecht, The Netherlands

<sup>4</sup>Harvard-Smithsonian Center for Astrophysics, Cambridge, MA 02138, U.S.A.

<sup>5</sup>Warsaw University Observatory, Al. Ujazdowskie 4, 00-478, Warsaw, Poland

<sup>6</sup>Max-Planck-Institut für extraterrestrische Physik, 85748 Garching, Germany

<sup>7</sup>University of California, 601 Campbell Hall, Berkeley, CA 94720

Received September 15, 1996; accepted March 16, 1997

## ABSTRACT

**Aims.** In order to discover new X-ray transients, the data taken by XMM-Newton as it slews between targets are being processed and cross-correlated with other X-ray observations.

**Methods.** A bright source, XMMSL1 J060636.2-694933, was detected on 18 July 2006 at a position where no previous X-ray source had been seen. The XMM-Newton slew data, plus follow-up dedicated XMM-Newton and Swift observations, plus optical data acquired with the Magellan Clay telescope, and archival All-Sky Automated Survey (ASAS) data were used to classify the new object, and to investigate its properties.

**Results.** No XMM-Newton slew X-ray counts are detected above 1 keV and the source is seen to be over five hundred times brighter than the ROSAT All-Sky Survey upper limit at that position. The line-rich optical spectrum acquired with the Magellan telescope allows the object to be classified as an A<sub>0</sub> auroral phase nova, and the soft X-ray spectrum indicates that the nova was in a super-soft source state in the X-ray decline seen in the follow-up X-ray observations. The archival ASAS data suggests that the nova at onset (Oct 2005) was a 'very fast' nova, and an estimate of its distance is consistent with the nova being situated within the LMC.

**Conclusions.** With the discovery presented here of a new classical nova in the LMC, it is clear that XMM-Newton slew data are continuing to offer a powerful opportunity to find new X-ray transient objects.

**Key words.** Novae – Stars: individual: XMMSL1 J060636.2-694933 – Surveys – X-rays: general

## 1. Introduction

The publicly available XMM-Newton slew data covers to date around 35% of the sky. The soft band (0.2–2 keV) sensitivity limit of the slews ( $6 \times 10^{-13}$  ergs cm<sup>-2</sup> s<sup>-1</sup>) is close to that of the ROSAT All-Sky Survey (RASS; Voges et al. 1999), and in the medium (2–12 keV) band, the slew data goes significantly deeper ( $4 \times 10^{-12}$  ergs cm<sup>-2</sup> s<sup>-1</sup>) than all other previous large area surveys. Over 7700 individual sources have so far been detected to a positional accuracy of 8". For details on the the construction and characteristics of the first released XMM-Newton slew survey catalogue, see Saxton et al. (2008). For details of the initial science results from the slew survey, see Read et al. (2006).

The comparison of XMM-Newton slew data with the RASS is now giving, for the first time, the opportunity to find exotic, extreme high-variability X-ray bursting objects, e.g. tidal disruption candidates (Esquej et al. 2007), and also Galactic novae, flare stars, and flaring white dwarfs, plus eclipsing binaries, AGN and blazars. It is only with such a large-area survey as the XMM-Newton Slew Survey, that transient events as these have a chance of being caught.

One such rare event, XMMSL1 J060636.2-694933, which we here show to be a new Classical Nova, was discovered in an XMM-Newton slew from 18th July 2006 at a very high count rate of 23.3 ct s<sup>-1</sup> (EPIC-pn: 0.2–2 keV).

Classical novae (see Bode & Evans 2008 for a review) occur in interacting binary systems consisting of a white dwarf primary star and a lower-mass secondary star. The nova itself is a cataclysmic nuclear explosion caused by the accretion of

material (via Roche Lobe overflow or wind accretion) from the secondary star onto the surface of the white dwarf; here the pressure and temperature at the base of the accreted material becomes sufficient to trigger a thermonuclear runaway. A recent review of the thermonuclear processes powering classical novae can be found in Starrfield et al. (2008). The accreted material is partially expelled, obscuring the X-ray emission from the surface of the white dwarf. At later stages, the ejected material expands further and becomes optically thin, revealing the nuclear burning on the surface of the white dwarf. This emission peaks in the soft X-ray regime and it is known as the super-soft source (SSS) state (Krautter 2008). Models of the classical nova SSS state can be found in Tuchman & Truran (1998) and Sala & Hernanz (2005).

Though many classical novae have been observed in X-rays in their SSS states (Ness et al. (2007) for example discuss several examples observed with Swift), it is in the optical band, early in their outbursts, that classical novae are almost always discovered. This is because they are intrinsically optically bright and easily found in inexpensive wide-area shallow surveys. XMMSL1 J060636.2-694933 is very unusual therefore in that it has been discovered, as we shall see, later in its evolution, in the SSS X-ray state.

In this paper we describe the XMM-Newton slew observations (Section 2), and the follow-up X-ray observations by the Swift XRT (Section 3) and XMM-Newton (Section 4). Multiwavelength observations with Swift-UVOT, Magellan and ASAS are described in Section 5. We then present a discussion of the results (Section 6), and conclusions.

## 2. XMM-Newton slew observations

XMMSL1 J060636.2-694933 was discovered in XMM-Newton slew 912100003 from revolution 1210 on 18th July 2006. Details of the standard XMM-Newton slew data reduction and analysis used, plus the source-searching and catalogue cross-correlation etc., are presented in Saxton et al. (2008).

The source passed through the EPIC-pn detector in 14 s, at a small off-axis angle, such that an effective vignetting-corrected soft band (0.2–2 keV) exposure time of 9.8 s was achieved. A total of 229 source counts lie within a radius of 20", yielding a (EPIC-pn: 0.2–2 keV) count rate of 23.4 ct s<sup>-1</sup>.

The source is seen to have no cross-correlation identifications in the RASS, and no other multiwavelength candidates within 30" in Simbad<sup>1</sup>, NED<sup>2</sup>, and HEASARC<sup>3</sup>. The position of the source in the sky is such that it lies apparently at the outer eastern edge of the LMC.

XMM-Newton has slewed over this region of sky a number of times, and though nothing was detected in previous slews from 7th November 2001 and 12th January 2004, the source was seen again on 28th September 2006 (rev. 1246, 72 days after the rev. 1210 discovery), at the same position, but at a reduced flux level (3.8 ct s<sup>-1</sup>; EPIC-pn: 0.2–2 keV). i.e. it had reduced in flux by a factor of  $\approx 6$  in 72 days. XMM-Newton has

not slewed over this area of sky since rev. 1246. Details of the relevant XMM-Newton slews, together with the (0.2–2 keV) EPIC-pn source position, detected source counts, count rate and detection likelihood are given in Table 1.

The fact that XMMSL1 J060636.2-694933 is detected in the total-band (0.2–12 keV) and the soft-band (0.2–2 keV), whilst effectively zero counts are seen in the hard-band (2–12 keV), is immediately indicative of the source being very soft.

The moderately high count rate indicates that the spectrum is affected by pile-up (the on-axis limit is 6 ct s<sup>-1</sup> for EPIC-pn full-frame mode<sup>4</sup>). This distorts the spectrum and makes quantitative spectral analysis of the slew data difficult. We minimized these effects by following the standard procedure, i.e. ignoring the central part of the Point Spread Function (PSF), and extracted an event spectrum (containing single and double events) of the source from within an annulus of 5"–30" radius, centred on the source position. Unresolved problems associated with the motion of sources across the detector still exist within slew data, and approximations currently have to be made when calculating the associated effective area and detector response matrix files. In order to perform qualitative spectral analysis, an effective area file was generated by averaging the individual core-removed effective area files at 9 different positions along the detector track made by the source. This accounts for the removal of the piled-up core, and takes the vignetting and PSF variations into account to a good approximation. Individual BACKSCAL values have been set by hand, as have the EXPOSURE values, estimated by calculating the distance travelled by the source in detector coordinates and finding the time taken to do this, given a 90 deg hr<sup>-1</sup> slew speed, then subtracting the appropriate fractions for chip gaps and bad pixels. For the response matrix, we used the equivalent canned detector response matrix for the vignetting-weighted average source position, for single plus double events and for full-frame mode: epn\_ff20\_sdY6\_v6.9.rmf. A background spectrum was extracted from a much larger circular region close to the source and at a similar off-axis angle.

To fit the slew spectral data, and indeed all the high-energy spectra in the present paper, the XSPEC<sup>5</sup> spectral fitting package has been used. As  $\chi^2$  minimization is not valid when fitting spectra of low statistical quality, for the fitting of the slew spectrum (and all the spectral fitting in the present paper), C-statistics have been used. To take into account the absorbing column along the line of sight, the *wabs* model with the *wilm* cosmic abundance table (Wilms et al. 2000) has been used throughout the paper. All the errors quoted in the present paper are 90% confidence intervals, unless otherwise stated.

The rev. 1210 slew spectrum shows that the source is very soft, and appears consistent with a  $63_{-10}^{+12}$  eV black body, absorbed by a hydrogen column density of  $8.2_{-4.1}^{+5.4} \times 10^{20}$  cm<sup>-2</sup>. The fit is good, with a P-statistic value of 0.11, obtained via the XSPEC *goodness* command for this fit, based on 5000 random simulations. The best-fit hydrogen column is equal

<sup>1</sup> <http://simbad.u-strasbg.fr/simbad/>

<sup>2</sup> <http://nedwww.ipac.caltech.edu/index.html>

<sup>3</sup> <http://heasarc.gsfc.nasa.gov/>

<sup>4</sup> [http://xmm.esac.esa.int/external/xmm\\_user\\_support/documentation/uhb\\_2.5/index.html](http://xmm.esac.esa.int/external/xmm_user_support/documentation/uhb_2.5/index.html)

<sup>5</sup> <http://heasarc.gsfc.nasa.gov/docs/xanadu/xspec/>

**Table 1.** Details of the four XMM-Newton Slew observations and the single (Rev. 1378) dedicated XMM-Newton pointed observation. XMM-Newton revolution, date and observation ID are tabulated, together with the 0.2–2.0 keV X-ray properties of XMMSL1 J060636.2-694933; position, background-subtracted counts, exposure, count-rate, and detection likelihood. For the Rev. 1378 dedicated observation, these properties are given for all the EPIC cameras combined. For the slew observations, only the EPIC-pn values are given. In the first two slews the source was not detected, and upper limits are shown in the table.

Rev	Date (UT)	Obs. ID	RA(J2000)	Dec(J2000)	Counts	Exposure (s)	Count rate (s <sup>-1</sup> )	Lik.
351 (slew)	07/11/01	9035100003			<3.6	8.8	<0.41	<~8
750 (slew)	12/01/04	9075000003			<3.2	17.3	<0.18	<~8
1210 (slew)	18/07/06	9121000003	06:06:36.2	-69:49:33	228.8±14.1	9.8	23.4±1.4	1777.1
1246 (slew)	28/09/06	9121460003	06:06:36.5	-69:49:38	12.9±2.4	3.4	3.8±0.7	54.7
1378 (pointed)	19/06/07	0510010501	06:06:36.5	-69:49:37	1511.0±44.8	8940.0	0.20±0.01	4630.4

to the full Galactic hydrogen column in the direction of the source ( $8.0 \pm 1.1 \times 10^{20} \text{ cm}^{-2}$ ; Dickey & Lockman, 1990, calculated via the FTOOL *nh*<sup>6</sup>). The slew spectrum, plus the best fit simple black body model and the deviations from the model, are shown in Fig. 1. The observed count rate corresponds to a (0.2–2 keV) flux, corrected for the removal of the saturated PSF core, of  $4.8^{+2.7}_{-1.6} \times 10^{-11} \text{ ergs cm}^{-2} \text{ s}^{-1}$  (an increase in flux over the RASS upper limit, assuming the same spectral model, by a factor of more than 500).

Simple power-law, thermal Bremsstrahlung, and other optically thin hot plasma models are unable to fit the spectrum adequately well. Given that we later are able to identify the source as a nova (Section 5.2), then the black-body model will likely be a good approximation. Furthermore, as we have obtained here a moderate number of slew counts, the more physically realistic, though more complex atmosphere model for CO white dwarfs of MacDonald & Vennes (1991), provided by K. Page (private communication), was attempted. This model, used e.g. to model the nova V1974 Cyg (Balman et al. 1998), yielded a marginal fit (and not formally a more statistically significant fit; P-statistic = 0.03, based on 5000 random simulations), with an effective temperature of  $70^{+8}_{-6} \text{ eV}$ , an  $N_{\text{H}}$  of  $3.7^{+3.2}_{-2.5} \times 10^{20} \text{ cm}^{-2}$ , and a PSF-corrected (0.2–2 keV) flux of  $4.5^{+1.3}_{-1.8} \times 10^{-11} \text{ ergs cm}^{-2} \text{ s}^{-1}$ . Note that a smaller  $N_{\text{H}}$  (though perhaps still consistent with the full Galactic hydrogen column) is now obtained using the white dwarf atmosphere model. (Note that the MacDonald & Vennes (1991) ONe white dwarf atmosphere model was also attempted, but yielded a marginally worse fit than the CO white dwarf atmosphere model; only the CO atmosphere model has been used in the subsequent analysis).

It is well known (e.g. Krautter et al. 1996) that, because of the energy-dependent opacity in the white dwarf atmosphere, fits to super soft source novae spectra with black body models give larger fluxes and lower temperatures than atmosphere models fit to the same spectra, and this is seen in the present case. Thus the black body model requires a larger  $N_{\text{H}}$  to fit the same data than the atmosphere model, as is seen.

The model normalizations, corrected for the removal of the saturated PSF core, can be used to derive an approximate distance to the source. If we assume a typical emitting region for the white dwarf atmosphere to be of spherical radius  $10^9 \text{ cm}$ , then, for the black body model, this distance turns out to be

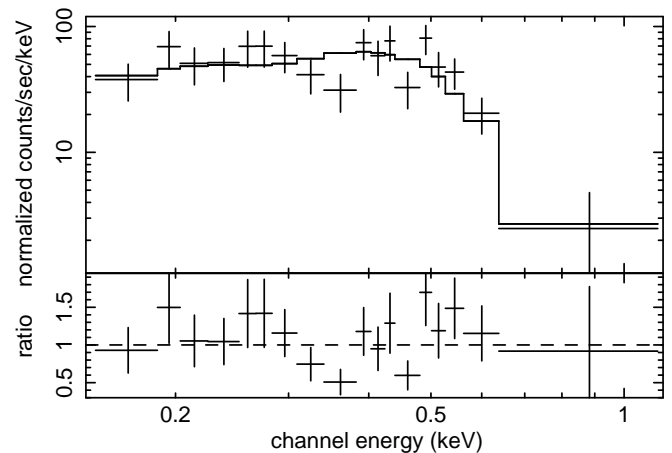


**Fig. 1.** XMM-Newton Slew spectrum of XMMSL1 J060636.2-694933 from XMM-Newton revolution 1210. The data points (crosses; adjacent data bins having been grouped together for the plot to have a significance of at least 3) have been fitted with a black body model ( $kT=63 \text{ eV}$ ; see text). The solid line shows the best fit to the spectrum. The ratio of the data to the best fit model is shown in the lower panel.

$20^{+31}_{-10} \text{ kpc}$ . The effects discussed above however can lead to usage of the black body model giving rise to an underestimation of the distance. For the white dwarf atmosphere model, a larger distance of  $71^{+27}_{-23} \text{ kpc}$  is obtained. Both estimates are consistent with the distance to the LMC ( $\sim 50 \text{ kpc}$ , see Section 6), and assuming a distance of 50 kpc, the black body derived flux corresponds to a (pile-up corrected) 0.2–2 keV X-ray luminosity of  $1.4^{+0.8}_{-0.5} \times 10^{37} \text{ ergs s}^{-1}$ .

### 3. Swift XRT X-ray observations

We requested and received a prompt observation with Swift of this source before it moved out of the Swift visibility window in April 2007. We received over 14 ksec of Swift-XRT time in 7 separate observations and the details of these observations are listed in Table 2. All of the observations were in photon counting mode and none of the observations showed any times of significant high-BG flux. In none of the observations did the source position coincide with any of the dead (micrometeorite-induced) detector columns. The analysis has

<sup>6</sup> <http://heasarc.gsfc.nasa.gov/lheasoft/ftools/fhelp/nh.txt>

**Table 2.** Details of the Swift-XRT observations (observation ID, observation date and cleaned exposure time) are tabulated, together with the total (0.2–2.0 keV) background-subtracted counts and count rate from XMMSL1 J060636.2-694933 (see text).

ID	Date (UT)	Exp. (s)	Counts	Count rate ( $s^{-1}$ )
00030895001	28/02/07	1955	23.9 $\pm$ 5.1	0.0122 $\pm$ 0.0026
00030895002	07/03/07	1796	15.8 $\pm$ 4.2	0.0088 $\pm$ 0.0024
00030895003	08/03/07	1651	10.9 $\pm$ 3.6	0.0066 $\pm$ 0.0022
00030895004	08/03/07	2547	20.6 $\pm$ 4.8	0.0081 $\pm$ 0.0019
00030895005	10/03/07	2550	29.5 $\pm$ 5.7	0.0116 $\pm$ 0.0022
00030895006	20/03/07	552	8.6 $\pm$ 3.2	0.0156 $\pm$ 0.0057
00030895007	22/03/07	3391	24.4 $\pm$ 5.4	0.0072 $\pm$ 0.0016

been performed using HEASOFT v6.1.2. The individual XRT observations were astrometrically-corrected and then stacked to ascertain a best Swift-XRT position – this was found to be 06 06 37.00 -69 49 33.9 (with a 90% error radius of 4.0''). Source counts were then extracted from each observation from a circle of radius of 40'' at this position. Background counts were extracted from each observation from large-radius off-source circles close to the source position. Source counts and count rates for the individual XRT observations are given in Table 2.

The observation naturally fell into three time-separated groups, those of obs. 1, obs. 2-5 and obs. 6-7. A similar analysis applied to these groups (where the statistics are improved) gives rise to source counts and count rates of 76.7 $\pm$ 9.3 counts and 0.0090 $\pm$ 0.0011 ct  $s^{-1}$  (for obs. 2-5), and 33.0 $\pm$ 6.2 counts and 0.0084 $\pm$ 0.0016 ct  $s^{-1}$  (for obs. 6-7). (Analysis of all the data together yields 133.6 $\pm$ 12.3 counts and 0.0092 $\pm$ 0.0009 ct  $s^{-1}$ ).

A spectrum was extracted from all the Swift-XRT data from a 40'' radius circle, using grades 0–12, centred on the Swift-XRT position. A background spectrum was extracted again from all the Swift-XRT data, from large-radius off-source circles close to the source position. An ARF file was created using *xrtmkarf* and the appropriate RMF (swxpc0to12\_20010101v008.rmf) from the Swift-XRT Calibration Database was obtained.

Standard spectral models were again fit to the spectral data using XSPEC. Again, C-statistics were used, as was the *wabs* absorption model with the *wilm* cosmic abundance table. It was again obvious that only a very soft spectrum would be appropriate for the data, and the only simple model that was able to fit the data adequately was a black-body model of temperature  $kT=59^{+14}_{-10}$  eV, with an absorbing hydrogen column of  $9.5^{+5.0}_{-3.9}\times 10^{20}$   $cm^{-2}$ . No sufficiently constrained parameters could be obtained using the CO white dwarf atmosphere model (MacDonald & Vennes 1991). The Swift-XRT spectrum, together with the best-fit black body model is shown in Fig. 2. The corresponding (0.2–2.0 keV) flux is  $2.7^{+0.7}_{-1.2}\times 10^{-13}$  ergs  $cm^{-2}$   $s^{-1}$  (i.e. a reduction by more than a factor 100 from the XMM-Newton slew discovery flux), and the X-ray luminosity, for the assumed distance of 50 kpc, is  $8.0^{+2.2}_{-3.5}\times 10^{34}$  ergs  $s^{-1}$ .

A cautious estimate of the size of the emitting region can be obtained from the model normalization; the assumed dis-

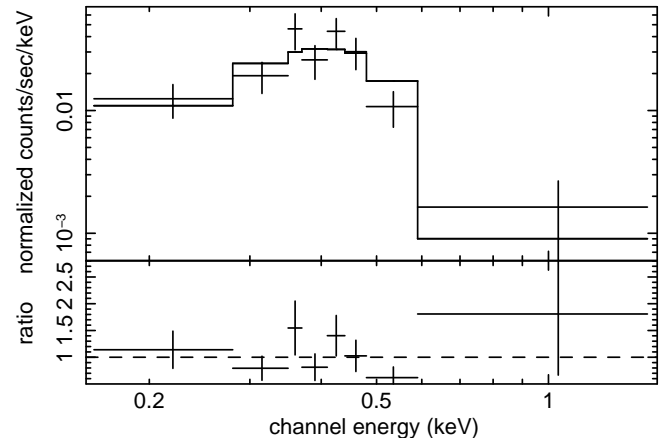


**Fig. 2.** Swift-XRT spectrum from XMMSL1 J060636.2-694933. The data points (crosses; adjacent data bins having been grouped together for the plot to have a significance of at least 3) have been fitted with a black body model ( $kT=59$  eV; see text). The source has faded by a factor of  $> 100$  since the XMM-Newton revolution 1210 slew discovery. The solid line show the best fit to the spectra. The ratio of the data to the best fit model is shown in the lower panel.

tance of 50 kpc yields a maximum radius of  $4.5\times 10^8$  cm (the fit normalization is essentially unconstrained at the lower bound). Though great care should be taken in interpreting this result, as the black body model is possibly overestimating the luminosity, this obtained radius is still consistent with that of moderately massive ( $>1.1M_{\odot}$ ) white dwarfs (Hamada & Salpeter 1961), i.e. the whole white dwarf surface may still be emitting at 59 eV.

#### 4. Dedicated XMM-Newton observations

We were granted an XMM-Newton Target of Opportunity (ToO) observation, once the source became again visible to XMM-Newton, and a 10 ks XMM-Newton EPIC observation was made on 19th June 2007 (see Table 1). All the XMM-Newton EPIC data, i.e. the data from the two MOS cameras and the single pn camera, were taken in full-frame mode with the thin filter in place. These data from the three EPIC instruments have been reprocessed using the standard procedures in XMM-Newton SAS (Science Analysis System) – v.7.1.0. Periods of high-background, of which there were very few, were filtered out of each dataset by creating a high-energy 10–15 keV lightcurve of single events over the entire field of view, and selecting times when this lightcurve peaked above 0.75 ct  $s^{-1}$  (for pn) or 0.25 ct  $s^{-1}$  (for MOS). This resulted in  $\approx 9.4(8.0)$  ks of low-background MOS(pn) data. Details of this dedicated XMM-Newton observation, together with source position, and (0.2–2 keV) all-EPIC combined (pn, MOS1, MOS2) detected source counts, count rate and detection likelihood are given in Table 1.

Source spectra, containing single and double events, were extracted from the datasets from circles (none of the data were now piled up) centred on the source position. An extraction radius, estimated from where the radial surface brightness profile

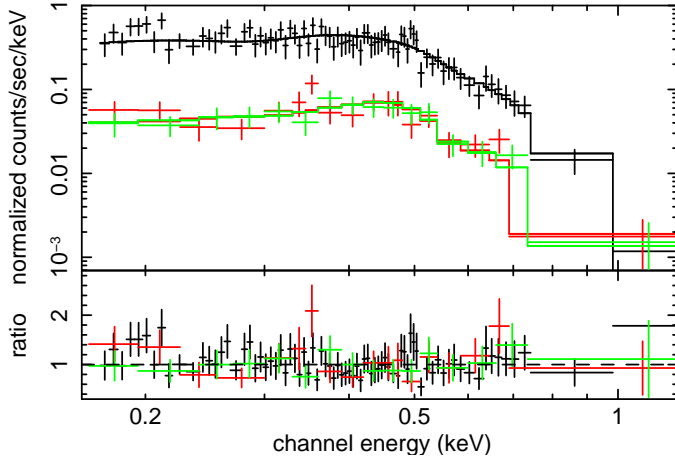


**Fig. 3.** XMM-Newton ToO spectrum from XMMSL1 J060636.2-694933. The data points (crosses; adjacent data bins having been grouped together for the plot to have a significance of at least 3)) have been fitted again with a black body model ( $kT=70$  eV) (see text). EPIC-pn data is shown in black, with EPIC-MOS1 in red and EPIC-MOS2 in green. The solid lines show the best fit to the spectra. The ratios of the data to the best fit model are shown in the lower panel.

was seen to fall to the surrounding background level, was set to  $30''$ . Background spectra were extracted from each cleaned dataset from a  $40''$ – $80''$  annulus centred on the source position. Point sources seen to contaminate these larger-area background spectra were removed from the background spectra to a radius of  $60''$ . ARF files were created for the source spectra, and were checked to confirm that the correct extraction area calculations had been performed. Finally RMF response files were generated.

Standard spectral models were again fit to the spectral data using XSPEC. Once again it was obvious that only a very soft model would fit the data; the only simple model that was able to fit the data well (a P-statistic = 0.17, based on 5000 random simulations) was a black-body model of temperature  $kT=70^{+3}_{-4}$  eV, with an absorbing hydrogen column of  $6.9^{+1.0}_{-1.6} \times 10^{20} \text{ cm}^{-2}$ . The spectrum, together with this best-fit model are shown in Fig. 3. The corresponding (0.2–2.0 keV) flux is only marginally less than the Swift-XRT value at  $2.2^{+0.8}_{-0.9} \times 10^{-13} \text{ ergs cm}^{-2} \text{ s}^{-1}$  and the X-ray luminosity (for the assumed distance of 50 kpc) is  $6.7^{+2.5}_{-2.8} \times 10^{34} \text{ ergs s}^{-1}$ .

Given that, in this XMM-Newton ToO observation, we had obtained a larger number of counts ( $\gtrsim 1500$  over the 3 EPIC cameras), the physically more realistic CO white dwarf atmosphere model (MacDonald & Vennes 1991) was also attempted. This yielded a marginal fit (and formally a no more statistically significant fit; P-statistic = 0.04, based on 5000 random simulations), with an effective temperature of  $73^{+3}_{-2}$  eV, and an  $N_{\text{H}}$  of  $3.4^{+0.8}_{-0.8} \times 10^{20} \text{ cm}^{-2}$ . Again, usage of the black body model results in a larger fitted  $N_{\text{H}}$  and a lower fitted temperature than with the atmosphere model.

As before, the model normalization can be used to obtain a cautious estimate of the size of the emitting region. For the assumed distance of 50 kpc, then the black body model re-

turns an emitting region radius of only  $1.3 \pm 0.2 \times 10^8 \text{ cm}$ . Again care should be taken, as this may be an overestimation, the black body model having perhaps overestimated the luminosity. For the white dwarf atmosphere model, a smaller radius of  $0.4 \pm 0.1 \times 10^8 \text{ cm}$  is obtained. Note further that the assumption of a larger distance (see Section 6) would result in a proportionally larger emitting radius. The range in allowed radius therefore is quite large, and it is not impossible for the whole of the white dwarf surface to be emitting at 70 eV. If this is the case, then the white dwarf would have to be at the high end of the mass range ( $> 1.2 M_{\odot}$ ; Hamada & Salpeter 1961). It may be the case then that we are at this point at, or close to the end of the SSS phase, where the effective temperature has reached a maximum (Sala & Hernanz 2005), as is tentatively seen in the spectral fitting results, and where the photospheric radius has reached a minimum, close to the white dwarf radius.

#### 4.1. X-ray variability

The full (XMM-Newton slew plus Swift-XRT plus XMM-Newton ToO) X-ray lightcurve of XMMSL1 J060636.2-694933 is shown in Fig. 4. The calculated (0.2–2.0 keV) flux values are shown plotted against the number of days since the rev.1210 XMM-Newton Slew discovery. The first two data points are the rev. 1210 and the rev. 1246 XMM-Newton Slew observations. Then the three nested Swift-XRT points are shown and finally the XMM-Newton ToO observation. The level of RASS upper limit is shown to the bottom left. The (0.2–2.0 keV) X-ray flux is seen to have dropped by more than two orders of magnitude in 230 days since the discovery, but is then seen to have levelled off for the next 120 days, at a level still  $\approx 3$  times that of the RASS. Finally, no evidence for any short-term variability (using time bins down to 100 s) is seen in the highest statistic continuous X-ray lightcurve (the  $\approx 8.0$  ksec background-filtered EPIC-pn lightcurve) obtained from the 19/06/07 XMM-Newton observation.

## 5. Multi-wavelength Follow-up

### 5.1. Swift UVOT

For the Feb/Mar 2007 Swift observations, we arranged for both the Swift UVOT-B filter and the UVOT-UVW2 filters to be used in an approximate exposure time ratio of 1:5, thus ensuring roughly equal numbers of counts in the two bands (though there is a spectral type dependency here). Swift UVOT images in these two filters of the area of sky around XMMSL1 J060636.2-694933 are shown in Fig. 5.

Prior to the Swift UVOT observations, a ‘best-guess’ to the possible candidate optical/IR counterpart would have been the USNO-A2.0 source 0150-04066298 (B mag: 17.4, R mag: 16.1), seen  $4''$  south of the XMM-Newton slew position. The UVOT images however immediately showed that the optically fainter source at position RA, Dec (J2000) = 06 06 36.4, -69 49 34.3 (error radius:  $0.5''$ ) was a very strong UVW2 source and very blue, and was very likely the true counterpart to XMMSL1 J060636.2-694933. (The UVW2 filter spans approximately  $800 \text{ \AA}$ , centred at  $\approx 1900 \text{ \AA}$ )

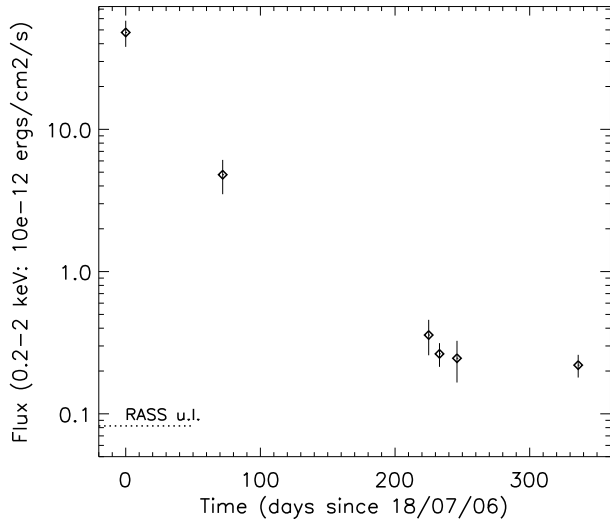


**Fig. 4.** The full X-ray lightcurve of XMMSL1 J060636.2-694933. Plotted are the calculated (0.2–2.0 keV) flux values versus time. The first point is the rev. 1210 XMM-Newton Slew observation, then the rev. 1246 XMM-Newton Slew observation. The three nested Swift-XRT points are shown next and finally the XMM-Newton ToO observation. The RASS upper limit is shown bottom left.

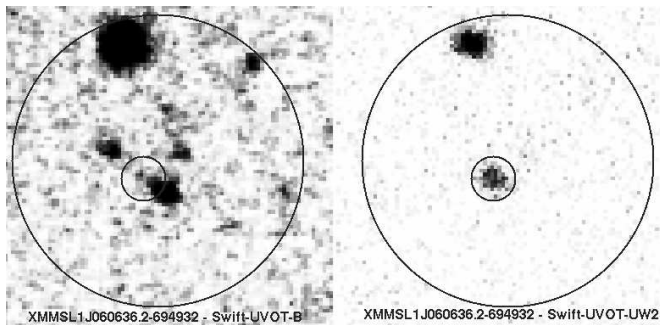


**Fig. 5.** Swift UVOT images of the field around XMMSL1 J060636.2-694933 from observation 00030895002. Left shows the UVOT B-filter and right shows the the UVOT UVW2-filter. The large circle is a 20'' radius circle around the XMM-Newton Slew position. The small circle in the UVW2 image around the bright source is reproduced in the B image, indicating that a faint optical source is also visible at this position.

The Swift UVOT pipeline processed data were analysed using the UVOT photometry package *uvotsource* released with FTOOLS<sup>7</sup>. This package performs aperture photometry on pre-specified source and background regions, accounting for photometric- (via PSF fitting) and coincidence loss- effects using the UVOT calibration files. Source counts were extracted using a 5'' radius aperture centred on the source, while for the background we used a 10'' radius aperture located in a nearby source-free region. We used a larger background aperture to effectively smooth over the modulo-8 fixed pattern noise present in UVOT observations and to improve the statistics of the background counts. Source counts were converted to UVOT UV-

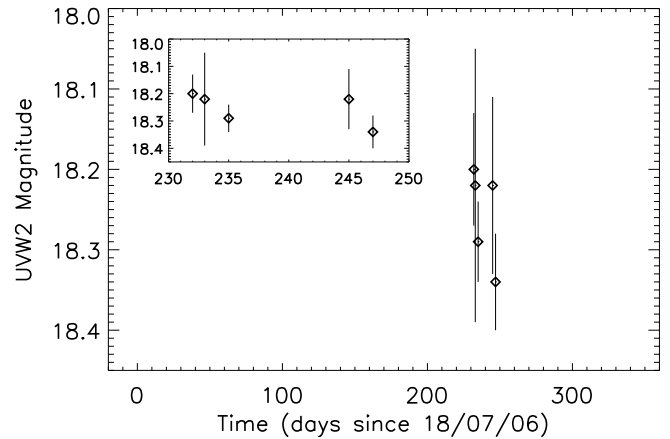


**Fig. 6.** Variation of the UVW2 magnitude of the bright UV source during the Swift observations. The same time axis as Fig.4 has been used to aid comparison, and a zoom is also shown. The UVW2 filter was only employed during observations 00030895002, 00030895004, 00030895005, 00030895006 & 00030895007 (hence the points span the dates 07/03/07 to 22/03/07). The errors here are 1- $\sigma$ .

magnitudes using the UVW2 zero-point calibration released with version 2.8 (Build 22) of the CALDB. The source is seen (see Fig. 6) to be roughly constant over the short duration of the Swift observations, with a suggestion of a decline towards the end. This is in keeping with the general form of the X-ray lightcurve (Fig. 4) at this time.

It is possible to include the UVOT-detected flux with the XRT spectrum described in Section 3. UVOT files, created using *uvot2pha* for the five observations (00030895002, 00030895004, 00030895005, 00030895006 & 00030895007) where the UVW2 filter was employed, were incorporated into *xspec*, along with the appropriate response file (*swuw2\_20041120v104.rsp*) from the Swift-XRT Calibration Database. We attempted to fit a single black-body spectrum to the Swift-XRT+UV data (again using C-statistics, the *wabs* absorption model and the *wilm* cosmic abundance table, plus the inclusion of the *xspec-redden* component to model the absorption in the UV band). The best fit however, with a much lower temperature of  $kT=36_{-4}^{+3}$  eV, is a very poor fit to the data; we obtain a *goodness* P-statistic value of 0.00, based on 5000 random simulations. This notwithstanding, a flux in the UVW2 (1.57–7.77 eV) band of  $3.5 \pm 0.2 \times 10^{-13}$  ergs cm<sup>-2</sup> s<sup>-1</sup> can be obtained, corresponding to a UVW2 luminosity, for the assumed distance of 50 kpc, of  $1.0 \pm 0.1 \times 10^{35}$  ergs s<sup>-1</sup>.

The very poor single black-body fit above, plus the large change in fitted temperature is strongly suggestive that a model other than, or in addition to the XRT-derived  $kT=59$  eV black body model (Section 3) should be used to describe the UVW2 data. As we have no UV data other than in the UVW2 filter, all that can be done is to apply the XRT-derived black body model to the UVW2+XRT data, and in doing this, a large flux excess with respect to the XRT-derived black body model is seen in the UVW2 band. This is shown in Fig.7. This excess in UV emission (most of the  $10^{35}$  ergs s<sup>-1</sup> discussed above) is likely

<sup>7</sup> [http://heasarc.nasa.gov/lheasoft/ftools/ftools\\_menu.html](http://heasarc.nasa.gov/lheasoft/ftools/ftools_menu.html)

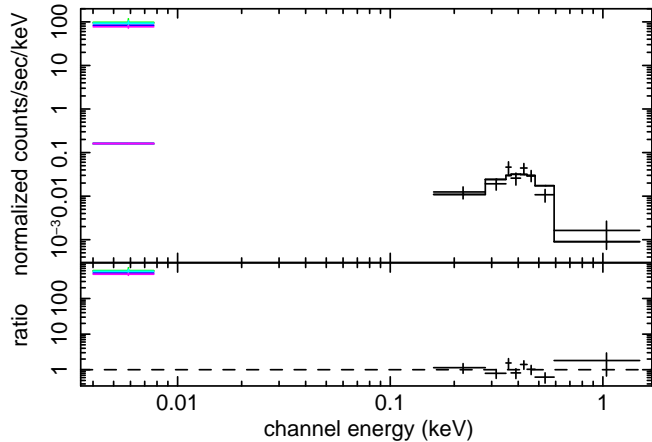


**Fig. 7.** Swift-XRT spectrum (black) from XMMSL1 J060636.2-694933, plus the best-fit black-body model to this spectrum (Section 3; Fig. 2), but extending into the UV to the Swift-UVOT UVW2 flux points (coloured) (see text). The data points are plotted such that adjacent data bins have been grouped together to have a significance of at least 3. The solid line show the best fit to the Swift-XRT spectrum. The ratio of the data to the best fit model is shown in the lower panel.

due to a combination of residual post-nova nuclear burning on the surface of the white dwarf, plus accretion in the disk, including from emission lines. The situation is likely to be rather complex, depending on the structure of both the ejecta and the accretion disk, and is beyond the scope of the present work, where we only have sparse UV data. For a review of the UV emission from classical novae, see Shore (2008).

## 5.2. Magellan optical observations

On Nov. 13, 14, and 15, 2007, XMMSL1 J060636.2-694933 was observed with the Low-Dispersion Survey Spectrograph 3 (LDSS3) mounted on the Magellan Clay telescope. Images were obtained through the Sloan  $g'$ ,  $r'$  and  $i'$  filters. On Nov. 15, 2007 conditions were photometric and the Landolt field RU 149A was observed to flux calibrate the data in the  $g'$ ,  $r'$  and  $i'$ -bands. The Landolt (1992) magnitudes of the standards were converted to Sloan magnitudes using the transformations presented in Smith et al. (2002). All the images were debiased and flatfielded using dome flatfield frames. We applied aperture photometry on each of the images using DAOPHOT in IRAF<sup>8</sup> to compute the instrumental magnitudes of the stars. Differential photometry of the optical counterpart to XMMSL1 J060636.2-694933 (marked by an arrow in Fig. 8) was performed with respect to the field star (marked with a 'c' in Fig. 8). This was the brightest isolated and unsaturated star common to all frames. The calibrated brightness of this comparison star is  $g' = 18.42 \pm 0.04$ ,  $r' = 17.85 \pm 0.06$  and  $i' = 17.58 \pm 0.07$ .

In addition to the imaging observations described above, we have obtained spectroscopic observations on Nov. 13, 14,

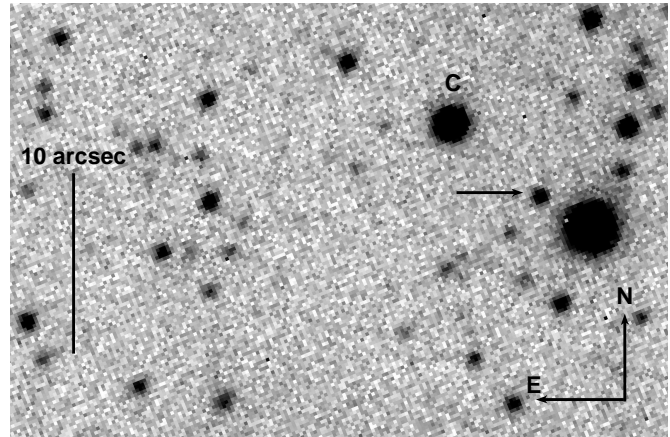


**Fig. 8.** Magellan Clay LDSS3 finder chart. The counterpart to XMMSL1 J060636.2-694933 (and the bright Swift-UVOT UVW2-filter source; Figs.5&6) is marked with an arrow. The comparison star is shown marked with a 'c'.

and 15, 2007 using the VPH All grism, which has 660 lines per mm, and employing a  $1''$  wide slit. This set-up provides a mean dispersion of  $2\text{\AA}$  per pixel. For a slit width of 1 arcsecond and a mean seeing close to  $1''$ , the mean spectral resolution is  $\approx 10\text{\AA}$ . On Nov. 13, 2007 we took 4 exposures of 450 s each, on Nov. 14, 2007 we took 2 exposures of 900 s each, and on Nov. 15, 2007 we took one 1200 s exposure with the slit at the parallactic angle. The spectra were bias and flatfield corrected, and extracted in IRAF. The instrumental response was corrected using the spectrophotometric flux calibrators LTT 3218 (Nov. 13), H600 (Nov. 14) and LTT 9293 (Nov. 15). Significant differences in the flux around  $H\alpha$  are apparent with the flux being 50% higher during the Nov. 15, 2007 with respect to the Nov. 13, 2007 observations. Since there is no evidence for brightening in the  $r'$  images we attribute the difference to the fact that the source was not observed at the parallactic angle on Nov. 13 and 14, 2007. We exported the one dimensional spectra to the spectral analysis software package MOLLY for further analysis.

We have averaged all spectra (see Fig. 9). We find several strong emission lines. The strongest of these emission lines are best interpreted as due to [OIII] 4958.9Å and 5006.9Å, He II at 4685.8Å and a blend of the  $H\alpha$  plus the [NII] at 6548.1Å and 6583.4Å, lines found often in novae (Williams 1992). In this case the main [OIII] lines appear redshifted by approximately  $2000\text{ km s}^{-1}$ . We interpret this as due to clumpy outflows in the nova shell. The integrated light from different outflowing parts can also explain the substructure that is present in the [OIII] lines. The outflow velocities that we obtain for the  $H\alpha$  and  $H\beta$  lines is  $\approx 350\text{ km s}^{-1}$ , hence less than that for the [OIII] lines. Note that, if XMMSL1 J060636.2-694933 does reside within the LMC, then the systematic line-of-sight recession velocity of the LMC,  $262 \pm 3.4\text{ km s}^{-1}$  (van der Marel et al. 2002), should be taken into account; i.e. a good fraction of the observed  $H\alpha$  and  $H\beta$  recession would then be due to the recession of the LMC itself.

<sup>8</sup> IRAF is distributed by the National Optical Astronomy Observatories

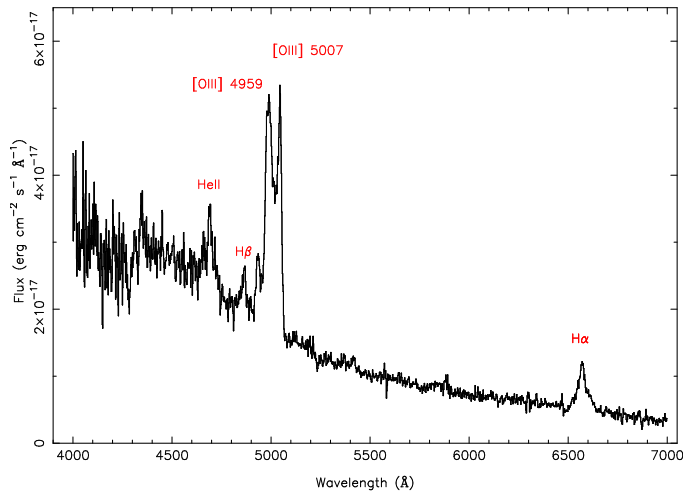


**Fig. 9.** Magellan Clay averaged optical spectrum of the optical source associated with XMMSL1 J060636.2-694933. The flux scaling is approximate. The prominent strong emission lines are marked (see text).

### 5.3. Long-term Optical light curve

Analysis of archival robotic optical survey data from 3-minute CCD exposures (pixel size  $14''.8$ ), obtained with a 70 mm (200 mm focal length)  $f/2.8$  telephoto lens in the course of the All Sky Automated Survey (ASAS; Pojmanski 2002) show that the visual magnitude of this source rose from  $m_V \gtrsim 14$  to  $m_V \approx 12$  between Sep. 18, 2005 and Sep. 30, 2005, and then declined rapidly thereafter (see Fig. 10). ASAS did not detect any significant emission from the source after around November 2005, the source having dimmed below the limiting magnitude of ASAS.

The decline from the brightest data point ( $\approx 2.2$  magnitudes in 10 days, then a further  $\sim 1.3$  magnitudes in 46 days) suggests that this is a nova of the ‘very fast’ speed class (Warner 1995, Downes et al. 2001). We estimate that the time that the light curve takes to decline 2 magnitudes below maximum observed brightness is  $8 \pm 2$  days (see Section 6).

## 6. Discussion

The optical spectrum, showing lines of [OIII] 4958.9Å and 5006.9Å, He II at 4685.8Å and a blend of the H $\alpha$  plus [NII] at 6548.1Å and 6583.4Å suggests that XMMSL1 J060636.2-694933 was a nova, observed (in Nov 2007) in the late A<sub>0</sub> auroral phase. The fact that the observed [OIII] lines are not in the more usual, optically thin 3:1 ratio, can be explained in terms of a clumpy outflow scenario, whereby individual clumps of both rest-frame and redward-shifted material are observed, and the superposition of these account for the observed [OIII] ratio (note further that density enhancements can change observed [OIII] ratios to more like  $\sim 1:1$ ). Clumps of material are often seen in nova ejecta (e.g. Shara et al. 1997), and outflows of speeds around  $2000 \text{ km s}^{-1}$  are not uncommon in novae (e.g. in nova LMC 1991; Schwartz et al. 2001).

XMMSL1 J060636.2-694933 was likely at its onset (in Oct 2005) a very fast, Fe II nova (Section 3 and Williams et al.

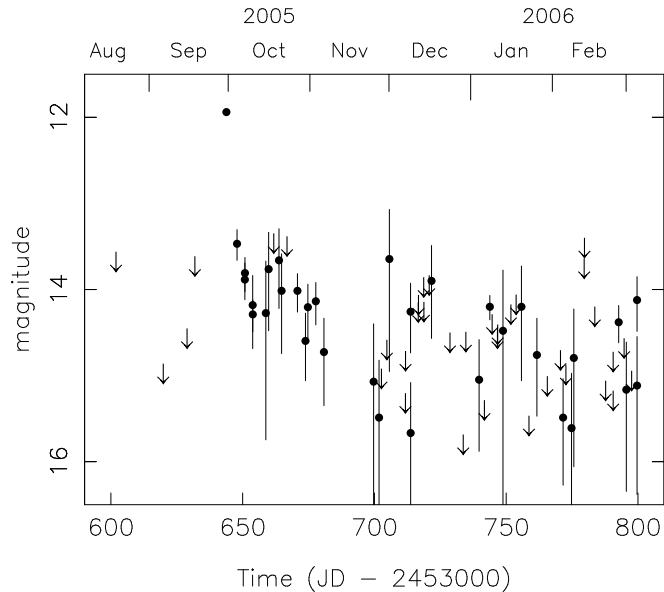


**Fig. 10.** All Sky Automated Survey V-band magnitudes of the optical counterpart to XMMSL1 J060636.2-694933, during outburst (late September 2005) and afterwards.

1991; Williams et al. 1994). An accurate classification now however is not possible, so late after maximum brightness. The soft ( $kT_{\text{eff}} \approx 60\text{--}70 \text{ eV}$ ) X-ray spectrum indicates that the nova was in a super-soft source (SSS) state (Krautter 2008) during its discovery (in July 2006), and throughout its X-ray decline (by more than two orders of magnitude) in the observations of Sept 2006, March 2007 and June 2007. Such a state originates from nuclear burning on the surface of the white dwarf, and measurements of the intensity, duration, and temperature can be used to estimate the distance to the nova and the mass of the white dwarf (e.g. Balman et al. 1998; Lanz et al. 2005). Indeed, we believe (Section 4) that the white dwarf within XMMSL1 J060636.2-694933 may be quite massive ( $> 1.2 M_{\odot}$ ).

As discussed earlier, classical novae are almost always discovered optically in the early phases of their outbursts. XMMSL1 J060636.2-694933 is very unusual therefore in that it has been discovered first in X-rays. As such, it is useful to compare it with XMMSL1 J070542.7-381442 (also known as V598 Pup; Read et al. 2008), another nova recently discovered (in X-rays) in the XMM-Newton slew survey. With a peak  $m_V$  of  $\lesssim 12$ , XMMSL1 J060636.2-694933 is not a particularly bright nova (c.f. V598 Pup, which reached an  $m_V$  of  $\lesssim 4$ ), and so it is not surprising that it went unnoticed, only being discovered in X-rays during the later (here 291 days after the outburst), optically thin nebular phase, when classical novae are typically observed as soft X-ray sources. Though this delay should be taken as an upper limit, it is long when compared to V598 Pup ( $\lesssim 127$  days), but may instead be more similar to the delays of  $\sim 200$  days seen in V1974 Cyg (Krautter et al. 1996),  $\sim 6$  months of V382 Vel (Orio et al. 2002), and 6–8 months of V1494 Aql (Drake et al. 2003). In their X-ray monitoring of optical novae in M31, Pietsch et al. (2007) detect 11 out of 34 novae in X-rays within a year after their optical outbursts. Seven novae are seen to be X-ray bright, several (3–9) years

after outburst, and three novae showed very short X-ray outbursts, starting within 50 days of outburst, but lasting only two to three months. XMMSL1 J060636.2-694933 therefore is not particularly unusual.

A method to estimate the distance to the nova is to use the relation between the absolute magnitude at maximum brightness and the time that the light curve takes to decline 2 magnitudes below maximum brightness,  $t_2$  (Della Valle & Livio 1995). We have no information over the 12 days between the data point of maximum brightness and the lower limit prior to this (Fig. 10), and therefore we have no exact outburst date, nor exact apparent magnitude at outburst. Assuming for the moment though that we have caught the outburst exactly in the Sep. 30, 2005 observation, then we can estimate (Sect. 5.3)  $t_2$  to be  $8 \pm 2$  days, and using this, we can estimate (Della Valle & Livio 1995) the absolute magnitude at maximum brightness  $M_V$  to be  $-8.7 \pm 0.6$ . An absolute magnitude of  $M_V = -8.7$  implies a peak luminosity  $\sim 7$  times the Eddington luminosity for a  $1 M_\odot$  white dwarf. This is quite typical of novae.

With  $A_V = 0.39_{-0.09}^{+0.05}$  (90% error), as derived (Predehl & Schmitt 1995) from  $N_H = 6.9_{-1.6}^{+1.0} \times 10^{20} \text{ cm}^{-2}$  (from the highest statistic spectral fit; the XMM-Newton ToO observation), and with  $M_V = -8.7 \pm 0.6$ , and a peak  $m_V$  of 12.0, we can derive a distance to XMMSL1 J060636.2-694933 of  $115_{-30}^{+43}$  kpc. As discussed above however, we are unsure as to the exact outburst date and the maximum brightness at outburst. Our assumed peak  $m_V$  of 12.0 is almost certainly an underestimation. Although we have no information in the 12 days prior to Sep. 30, 2005, a simple linear extrapolation of the early October lightcurve back prior to Sep. 30, 2005 suggests that the actual peak  $m_V$  was somewhere between 9 and 12. The corresponding distance estimates are then between 29 and 115 kpc (with a mid-point  $m_V = 10.5$  value yielding a distance estimate of 58 kpc). Many methods have been used to estimate the distance to the LMC (e.g. Kovacs 2000, Nelson et al. 2000), but a value of around 50 kpc appears to be quite robust. Our distance estimate is certainly consistent with that of the LMC, though the errors are quite large. It does appear to be the case however, that our distance estimate places the source far outside of our own Galaxy. This, together with the source's position on the sky (at the eastern edge of the LMC) and the sizable ( $\sim$ Galactic) X-ray hydrogen column densities obtained from the spectral fits, suggest strongly that XMMSL1 J060636.2-694933 lies within the LMC itself. Note further that the (pile-up corrected) spectral model normalizations to the initial Slew discovery data (Sect. 2) also imply an approximate distance to XMMSL1 J060636.2-694933 of  $\sim 50$  kpc.

The source had, at the time of the slew detection, an absorbed (0.2–2 keV) X-ray flux of  $4.8_{-1.6}^{+2.7} \times 10^{-11} \text{ ergs cm}^{-2} \text{ s}^{-1}$ , corresponding to a 0.2–2 keV X-ray luminosity (at 50 kpc) of  $1.4_{-0.5}^{+0.8} \times 10^{37} \text{ ergs s}^{-1}$ . Assuming instead for the moment a distance more like 100 kpc (though this is thought to be well beyond the LMC, e.g. Kovacs 2000), then the (0.2–2 keV) X-ray luminosity of  $5.7_{-1.9}^{+3.0} \times 10^{37} \text{ erg s}^{-1}$  obtained is at the high end of the X-ray luminosities of classical SSS-phase novae discussed e.g. in Orio et al. (2002) and Ness et al. (2007). As discussed though, we have very likely missed the outburst peak, and as such, our more probable assumed distance of 50 kpc gives rise

to a more typical SSS-phase X-ray luminosity. The luminosities of  $7\text{--}8 \times 10^{34} \text{ erg s}^{-1}$ , obtained during the Swift and pointed XMM-Newton observations, are more typical of novae at later times, when the emission can also sometimes be described by a thermal plasma, rather than a black-body type spectrum, or a more mixed spectrum, due to the complex structure of the ejecta and the accretion disk (Krautter 2008, Shore 2008).

## 7. Conclusions

A bright X-ray source, XMMSL1 J060636.2-694933, was detected in an XMM-Newton slew on 18 July 2006 at a position where no previous X-ray source had been seen. The XMM-Newton slew data, plus follow-up dedicated XMM-Newton and Swift observations, plus optical imaging and spectroscopic data acquired with the Magellan Clay telescope and All-Sky Automated Survey (ASAS) data were used to classify the new object as a nova, and to examine its properties. The primary conclusions are as follows:

- The soft X-ray spectrum indicates that the nova was in a super-soft source (SSS) state at its discovery in July 2007 (XMM-Newton slew) and through its X-ray decline (by over two orders of magnitude) in September 2006 (XMM-Newton slew), March 2007 (Swift) and June 2007 (XMM-Newton).
- The Magellan optical spectrum (Nov 2007) of the source indicates that it was very likely then a nova in the late  $A_0$  auroral phase.
- The very fast optical decline (ASAS) during the nova's onset (Oct 2005), indicates that the initial nova was likely of speed class 'very fast'.
- The very fast speed, together with the absolute magnitude at maximum brightness and the X-ray absorption, give rise to a distance to the source far beyond our own Galaxy. The large distance, together with the source's position in the sky, at the eastern edge of the LMC, and the spectral information from the X-ray data, are very suggestive that the nova is situated within the LMC itself.
- Analysis of XMM-Newton slew data is continuing to provide a powerful means of finding new X-ray transient objects.

*Acknowledgements.* The XMM-Newton project is an ESA Science Mission with instruments and contributions directly funded by ESA Member States and the USA (NASA). The XMM-Newton project is supported by the Bundesministerium für Wirtschaft und Technologie/Deutsches Zentrum für Luft- und Raumfahrt (BMWi/DLR, FKZ 50 OX 0001), the Max-Planck Society and the Heidenhain-Stiftung. AMR and PE acknowledge the support of STFC funding, and PGJ of the Netherlands Organisation for Scientific Research. The ASAS project is supported by the N2030731/1328 grant from the MNiSzW. We thank the referee (G. Sala) for very useful comments and several references that have improved the paper notably. We thank Kim Page for providing the white dwarf atmosphere model, and we thank her and Graham Wynn for useful discussions. The use of the spectral analysis software package MOLLY written by Tom Marsh is also acknowledged. MM acknowledges support by a Miller Institute Research Fellowship during the time in which part of the work was completed.

## References

- Balman S., Krautter J., Oegelman H., 1998, *ApJ* 499, 395
- Bode M.F., Evans A., 2008, *Classical Novae*, Cambridge University Series 43, CUP
- Della Valle M., Livio M., 1995, 452, 704
- Dickey J.M., Lockman F.J., 1990, *ARA&A*, 28, 215
- Downes R.A., Duerbeck H.W., Delahodde C.E., 2001, *JAD*, 7, 6
- Drake J.J., et al., 2003, *ApJ* 584, 448
- Esquej P., Saxton R.D., Freyberg M.J., Read A.M., Altieri B., Sanchez-Portal M., Hasinger G., 2007, *A&A* 462, 49
- Hamada T., Salpeter E.E., 1961, *ApJ* 134, 683
- Kovacs G., 2000, *A&A*, 363, 1
- Krautter J., 2008, in *Classical Novae*, Eds. Bode M.F., Evans A., Cambridge University Series 43, CUP, p232
- Krautter J., Oegelman H., Starrfield S., et al., 1996, *ApJ* 456, 788
- Landolt A.U., 1992, *AJ*, 104, 340
- Lanz T., Telis G.A., Audard M., et al., 2005, *ApJ* 619, 517L
- MacDonald J., Vennes S., 1991, *ApJ*, 373, L51
- Nelson C.A., Cook K.H., Popowski P., Alves D.R., 2000, *AJ*, 119, 1205
- Ness J.-U., Schwartz G.J., Retter A., et al., 2007, *ApJ* 663, 505
- Orio M., Parmar A.N., Greiner J., et al., 2002, *MNRAS* 333, L11
- Pietsch W., Haberl F., Sala G., Stiele H., Hornoch K., Riffeser A., Fliri J., Bender R., Buehler S., Burwitz V., Greiner J., Seitz S., 2007, *A&A* 465, 375
- Pojmanski G. 2002, *Acta Astronomica*, 52, 397
- Read A.M., Saxton R.D., Esquej P., Freyberg M.J., Altieri B., 2006, *PASJ*, 58, No 6, 47
- Read A.M., Saxton R.D., Torres M.A.P., Esquej P., Kuulkers E., Jonker P.G., Osborne J.P., Freyberg M.J., Challis P., 2008, *A&A*, 482, L1
- Sala G., Hernanz M., 2005, *A&A*, 439, 1061
- Saxton R.D., Read A.M., Freyberg M.J., Esquej P., Altieri B., Bermejo D., 2008, *A&A*, 480, 611
- Schwarz G.J., Shore S.N., Starrfield S., Hauschildt P.H., Della Valle M., Baron E., *MNRAS* 320, 103
- Shara M.M., Zurek D.R., Williams R.E., Prialnik D., Gilmozzi R., Moffat A.F.J., 1997, *AJ* 114, 258
- Shore, S.N., 2008, in *Classical Novae*, Eds. Bode M.F., Evans A., Cambridge University Series 43, CUP, p194
- Smith J.A., Tucker D.L., Kent S., et al., 2002, *AJ*, 123, 2121
- Starrfield S., Iliadis C., Hix W.R., 2008, in *Classical Novae*, Eds. Bode M.F., Evans A., Cambridge University Series 43, CUP, p77
- Tuchman Y, Truran J.W., 1998, *ApJ*, 503, 381
- van der Marel R.P., Alves D.R., Hardy E., Suntzeff N.B., 2002, *AJ* 124, 2639
- Warner B., 1995, *Cataclysmic Variable Stars*, Cambridge
- Williams R.E., Hamuy M., Phillips M.M., et al., 1991, *ApJ*, 376, 721
- Williams R.E., 1992, *AJ*, 104, 725
- Williams R.E., Phillips M.M., Hamuy M., 1994, *ApJSS* 90, 297
- Wilms J., Allen A., McCray R., 2000, *ApJ* 542, 914
- Voges W., Aschenbach B., Boller T., et al., 1999, *A&A*, 349, 389